Hindawi
International Journal of Aerospace Engineering
Volume 2022, Article ID 6296770, 18 pages
https://doi.org/10.1155/2022/6296770

Research Article

Research on Three-Dimensional Integrated Guidance and Control Design with Multiple Constraints

Zhenhua Fu,[1] Kuanqiao Zhang ,[2] and Suochang Yang[3]

[1]*School of Automation, Beijing Institute of Technology, Beijing, China*
[2]*State Key Laboratory of Complex Electromagnetic Environment Effects on Electronics and Information System, Luoyang, China*
[3]*Army Engineering University, Shijiazhuang, China*

Correspondence should be addressed to Kuanqiao Zhang; zkuanqiao@163.com

Received 12 January 2022; Revised 25 May 2022; Accepted 17 June 2022; Published 18 July 2022

Academic Editor: Shaoming He

In this paper, a fixed-time convergence-integrated guidance and control (IGC) method is proposed, which considers terminal line-of-sight (LOS) angle constraint, full-state constraints, and input saturation. Firstly, an IGC design model considering the full coupling of three channels is constructed, and a fixed-time convergence disturbance observer is used to estimate and compensate the unknown disturbances in the model. Secondly, based on the fixed-time stability theory, sliding mode control, and backstepping control, a novel IGC scheme is carried out, and the second-order instruction filter is used to restrict the system states and control instructions. Furthermore, the fixed-time stability of the close-loop system is proved and the expression of convergence time upper bound is given. Finally, comparison simulation and Monte Carlo simulation verify the effectiveness and superiority of the proposed IGC algorithm.

1. Introduction

The guidance and control system (GCS) is the core system of missile. The classical GCS is designed individually, which includes guidance loop and control loop. In contrast, the IGC design scheme takes guidance loop and control loop as a whole. Since the IGC design method can take advantage of the coupling relationship between guidance system and control system, as well as the comprehensive information, such as the information on the relative motion of the missile and the target, the attitude angle, and overload of the missile, it can significantly enhance the missile performance compared with the classical scheme [1, 2].

There were many theories and methods for IGC scheme, including small gain theory [3], predictive control [4], variable structure control [5], adaptive control [6], and backstepping control [7]. Among them, backstepping control method was used widely. However, backstepping control had the problem that was called "exponential expansion," which was due to the need to differentiate the virtual control quantity multiple times. To overcome this problem, dynamic surface control was proposed and applied to IGC design [8]. The derivatives of virtual quantities were obtained by introducing a first-order filter. In [9], a 3D IGC scheme is proposed by using sliding mode control and backstepping control. The scheme used the Nussbaum function and an auxiliary system to solve the problem of input saturation. However, it was a three-channel independent design method. In [10], the dynamic surface control and barrier Lyapunov function were used in IGC design, and a neural network disturbance observer was applied to estimate the system interferences.

Many missiles, such as antitank missiles and antiaircraft missiles, can increase their warhead damage by controlling the terminal impact angles when attacking the target [11]. Therefore, terminal angle constraint such as LOS angle constraint can be considered in IGC design to improve the combat effectiveness of missile. In [12], a robust IGC design method with terminal LOS angle constraint was obtained based on dynamic inverse control, and the system uncertainties were restrained by introducing sliding mode control. The sign function was replaced by continuous high gain saturation function to solve the chattering problem inherent in sliding mode control. But it also changed the original structure of sliding mode control and reduced the robustness. In [13], an IGC scheme with terminal LOS angle constraint was designed based on dynamic surface control, and adaptive control was adopted to compensate system disturbances. However, dynamic surface control-based IGC design could only ensure that the system states converge asymptotically, but the missile attack time is limited.

Because of the aerodynamic structure limitation, the missile system state variables, such as attack angle and Euler angular rates, should change within certain ranges during the flight. In the meanwhile, because of the actuator physical limitation, the control ability generated by the actuator is limited. Taking pneumatic rudder as an example, both positive and negative rudder deflection angles have upper bounds. If rudder deflection angles and system state variables exceed the allowed ranges, the missile guidance and control performance will be negatively affected. Even the missile will be uncontrollable and unstable, leading to off-target [14]. Therefore, state constraints and control constraint should be considered in the IGC design. In [15], dynamic surface control was used to carry out an IGC system, and the model uncertainty and disturbance were estimated by a proposed finite-time convergence disturbance observer. In addition, the Nussbaum function was used to deal with the control constraint, which was also known as input saturation. In [16], aiming at state constraints, an IGC system was designed based on dynamic surface control and barrier Lyapunov function. In order to solve the state constraints, a saturation function was introduced into the design to ensure that the state variables did not change beyond the constraint ranges.

The above analysis shows that most of the literatures on IGC design research aim to solve unitary constraint problem, such as terminal LOS angle constraint, input saturation, state constraints, and finite-time convergence. However, the missile GCS was faced with a variety of constraints. As far as we know, there are few literatures dealing with the problems of input saturation, full-state constraints, terminal LOS angle constraint, and global finite-time convergence in 3D IGC scheme. For this issue, a fixed-time IGC algorithm for STT missile is proposed in this paper, which considers terminal LOS angle constraint, input saturation, and full-state constraints. The main contributions are as follows:

(a) A 3D IGC design model with multiple constraints is established rather than the single plane model established in [5]

(b) A sliding mode surface which can strictly converge in fixed-time is designed to solve terminal angle constraint rather than common asymptotic stability

(c) The second-order instruction filter is constructed to estimate the derivative of the virtual commands, which effectively relieve the computation burden in backstepping design, and guarantee virtual commands in prescribed ranges. Furthermore, an auxiliary system is designed to eliminate the tracking error of the filter

(d) Different from the general asymptotic or finite-time convergence IGC algorithms proposed in [15–17], a 3D IGC algorithm is proposed to achieve global fixed-time convergence in the presence of extern disturbances, terminal angle constraint, full-state constraints, and input saturation

2. Problem Description and Preliminaries

2.1. Problem Description. Figure 1 establishes the relative motion of missile and target in 3D inertial coordinate system $Oxyz$, where $Ox_4y_4z_4$ is the LOS coordinate system. M represent the missile and T represent target. ε is LOS elevation angle and η is the azimuth angle. R is relative distance of missile and target. Define $a_{\mathrm{m}_4} = [a_{\mathrm{m}x_4}\ a_{\mathrm{m}y_4}\ a_{\mathrm{m}z_4}]^{\mathrm{T}}$ and $a_{\mathrm{t}_4} = [a_{\mathrm{t}x_4}\ a_{\mathrm{t}y_4}\ a_{\mathrm{t}z_4}]^{\mathrm{T}}$ which are acceleration vectors of missile and target in $Ox_4y_4z_4$, respectively.

The missile and target relative motion equations [18] are

$$\begin{cases} 2\dot{R}\dot{\varepsilon} + R\ddot{\varepsilon} + R\dot{\eta}^2 \sin\varepsilon\cos\varepsilon = a_{\mathrm{t}y_4} - a_{\mathrm{m}y_4}, \\ -2\dot{R}\dot{\eta}\cos\varepsilon - R\ddot{\eta}\cos\varepsilon + 2R\dot{\varepsilon}\dot{\eta}\sin\varepsilon = a_{\mathrm{t}z_4} - a_{\mathrm{m}z_4}. \end{cases} \tag{1}$$

Define $a_{\mathrm{m}_2} = [a_{\mathrm{m}x_2}\ a_{\mathrm{m}y_2}\ a_{\mathrm{m}z_2}]^{\mathrm{T}}$, which is missile acceleration vector in ballistic coordinate system. It can be obtained from the missile dynamic equations as

$$\begin{cases} a_{\mathrm{m}y_2} = \dfrac{[P(\sin\alpha\cos\gamma_V + \cos\alpha\sin\beta\sin\gamma_V) + Y\cos\gamma_V - Z\sin\gamma_V - mg\cos\theta_{\mathrm{m}}]}{m}, \\ a_{\mathrm{m}z_2} = \dfrac{[P(\sin\alpha\sin\gamma_V + \cos\alpha\sin\beta\cos\gamma_V) + Y\sin\gamma_V + Z\cos\gamma_V]}{m}, \end{cases} \tag{2}$$

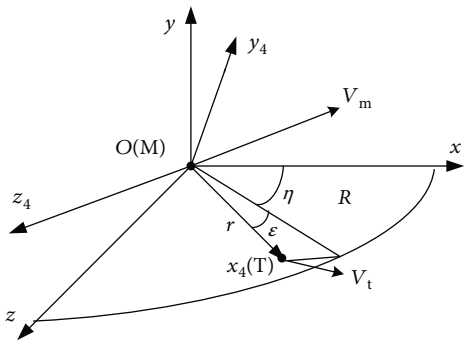

Figure 1: Relative motion of missile and target.

where m is missile mass, θ_m is fight path angle, α is attack angle, β is sideslip angle, γ_V is bank angle, Y is aerodynamic lift force, Z is lateral force, P is thrust force, and g is gravitational acceleration.

From the coordinate transformation, we can get

$$a_{m_4} = L(\eta,\varepsilon)L^{-1}(\psi_{Vm},\theta_m)a_{m_2},$$
$$L(\eta,\varepsilon) = \begin{bmatrix} \cos\varepsilon\cos\eta & \sin\varepsilon & -\cos\varepsilon\sin\eta \\ -\sin\varepsilon\cos\eta & \cos\varepsilon & \sin\varepsilon\sin\eta \\ \sin\eta & 0 & \cos\eta \end{bmatrix},$$
$$L(\psi_{Vm},\theta_m) = \begin{bmatrix} \cos\theta_m\cos\psi_{Vm} & \sin\theta_m & -\cos\theta_m\sin\psi_{Vm} \\ -\sin\theta_m\cos\psi_{Vm} & \cos\theta_m & \sin\theta_m\sin\psi_{Vm} \\ \sin\psi_{Vm} & 0 & \cos\psi_{Vm} \end{bmatrix}, \tag{3}$$

where ψ_{Vm} is the heading angle of missile.

The aerodynamic forces Y and Z are modeled as

$$\begin{cases} Y = C_y^\alpha \alpha QS + Y^{\delta_z} + d_Y, \\ Z = C_z^\beta \beta QS + Z^{\delta_y} + d_Z, \end{cases} \tag{4}$$

where Y^{δ_z} and Z^{δ_y} are lift force and lateral force produced by the rudder angles, C_y^α and C_z^β are aerodynamic coefficient with respect to α and β, $Q = \rho V_m^2/2$ is dynamic pressure, S stands for the reference area, ρ is atmospheric density, and d_Y and d_Z are the unknown bounded uncertainties including modeling error and model uncertainties, here treated as disturbance variables.

Since the rudder deflection angles contribute little to the aerodynamic forces, Y^{δ_z} and Z^{δ_y} can be regarded as small quantities [19].

In this paper, the IGC design applies only to the terminal guidance stage. Therefore, assuming that the missile flies without power and the flight speed is approximately invariant, the velocity change rate is regarded as interference. For STT missile, its required bank angle control is zero. So it can be assumed to be a small quantity, and $\sin(\gamma_V) \approx 0$ and $\cos(\gamma_V) \approx 1$. Define new state variables $x_1 = [\dot\varepsilon\ \dot\eta]^T$ and $x_2^\# = [\alpha\ \beta]^T$. Combined with (1) to (4), the relative motion equation in 3D space can be described as

$$\dot x_1 = f_1(x_1) + g_1(x_1)x_2^\# + d_1(t), \tag{5}$$

with

$$f_1(x_1) = \begin{bmatrix} -\frac{2\dot R}{R}\dot\varepsilon - \dot\eta^2\sin\varepsilon\cos\varepsilon + \frac{f(\theta_m)}{R}g\cos\theta_m \\ -\frac{2\dot R}{R}\dot\eta + 2\dot\varepsilon\dot\eta\tan\varepsilon + \frac{\sin\theta_m\sin(\eta-\psi_{Vm})}{R\cos\varepsilon}g\cos\theta_m \end{bmatrix},$$
$$g_1(x_1) = \begin{bmatrix} -\frac{f(\theta_m)}{mR}C_y^\alpha QS & -\frac{\sin\varepsilon\sin(\eta-\psi_{Vm})}{mR}C_z^\beta QS \\ -\frac{\sin\theta_m\sin(\eta-\psi_{Vm})}{mR\cos\varepsilon}C_y^\alpha QS & \frac{\cos(\eta-\psi_{Vm})}{mR\cos\varepsilon}C_z^\beta QS \end{bmatrix},$$
$$d_1 = \begin{bmatrix} \frac{a_{ty4}}{R} - \frac{d_Y f(\theta_m) + d_Z\sin\varepsilon\sin(\eta-\psi_{Vm})}{mR} \\ -\frac{a_{tz4}}{R\cos\varepsilon} - \frac{d_Y\sin\theta_m\sin(\eta-\psi_{Vm}) - d_Z\cos(\eta-\psi_{Vm})}{mR\cos\varepsilon} \end{bmatrix},$$
$$f(\theta_m) = \cos\theta_m\cos\varepsilon + \sin\theta_m\sin\varepsilon\cos(\eta-\psi_{Vm}). \tag{6}$$

As is well known that R is bounded, and target acceleration and aerodynamic parameters (Y^{δ_z}, Z^{δ_y}, d_Y, and d_Z) are bounded, so $d_1(t)$ is bounded.

According to missile dynamic equations [20], the missile control model can be described as

$$\begin{cases} \dot\alpha = -\omega_x\tan\beta\cos\alpha + \omega_y\tan\beta\sin\alpha + \omega_z - \dfrac{C_y^\alpha\alpha QS - mg\cos\theta_m}{mV_m\cos\beta} + \Delta_\alpha, \\ \dot\beta = \omega_x\sin\alpha + \omega_y\cos\alpha + \dfrac{C_z^\beta\beta QS}{mV_m} + \Delta_\beta, \\ \dot\gamma = \omega_x - \omega_y\tan\vartheta\cos\gamma + \omega_z\tan\vartheta\sin\gamma + \Delta_\gamma, \\ \dot\omega_x = \dfrac{\left(m_x^\alpha\alpha + m_x^\beta\beta + m_x^{\delta_x}\delta_x\right)QSL}{J_x} + \dfrac{J_y - J_z}{J_x}\omega_y\omega_z + \Delta_{\omega_x}, \\ \dot\omega_y = \dfrac{\left(m_y^\beta\beta + m_y^{\delta_y}\delta_y\right)QSL}{J_y} + \dfrac{J_z - J_x}{J_y}\omega_z\omega_x + \Delta_{\omega_y}, \\ \dot\omega_z = \dfrac{\left(m_z^\alpha\alpha + m_z^{\delta_z}\delta_z\right)QSL}{J_z} + \dfrac{J_x - J_y}{J_z}\omega_x\omega_y + \Delta_{\omega_z}, \end{cases} \tag{7}$$

where γ is roll angle, J_x, J_y, and J_z are the inertia components, ω_x, ω_y, and ω_z are Euler angular rates, m_x^α, m_z^α, m_x^β, m_y^β, $m_x^{\delta_x}$, $m_y^{\delta_y}$, and $m_z^{\delta_z}$ are moment aerodynamic coefficients with respect to α, β, δ_x, δ_y, and δ_z, which δ_x, δ_y, and δ_z are rudder angles, Δ_α, Δ_β, Δ_γ, Δ_{ω_x}, Δ_{ω_y}, and Δ_{ω_z} are external disturbances and modeling errors, and ϑ is missile pitch angle.

The missile terminal LOS angle constraint [21] can be described as

$$\varepsilon(t_f) = \varepsilon_d, \eta(t_f) = \eta_d, \tag{8}$$

where t_f is the guidance final moment and ε_d and η_d are expected terminal LOS angles.

Define new state variables $\mathbf{x}_0 = [\varepsilon - \varepsilon_d \ \eta - \eta_d]^T$, $\mathbf{x}_2 = [\alpha \ \beta \ \gamma]^T$, $\mathbf{x}_3 = [\omega_x \ \omega_y \ \omega_z]^T$, and $\mathbf{u} = [\delta_x \ \delta_y \ \delta_z]^T$. Combining with (5) and (7), the IGC design model with terminal LOS angle constraint is established as

$$\begin{cases} \dot{x}_0 = x_1, \\ \dot{x}_1 = f_1(x_1) + g_1(x_1)x_2^{\#} + d_1(t), \\ \dot{x}_2 = f_2(x_2) + g_2(\vartheta, x_2)x_3 + d_2(t), \\ \dot{x}_3 = f_3(x_2, x_3) + g_3 u + d_3(t), \end{cases} \tag{9}$$

with

$$f_2(x_2) = \begin{bmatrix} -\dfrac{C_y^{\alpha}\alpha QS - mg\cos\theta_m}{mV_m\cos\beta} \\ \dfrac{C_z^{\beta}\beta QS}{mV_m} \\ 0 \end{bmatrix},$$

$$g_2(\vartheta, x_2) = \begin{bmatrix} -\tan\beta\cos\alpha & \tan\beta\sin\alpha & 1 \\ \sin\alpha & \cos\alpha & 0 \\ 1 & -\tan\vartheta\cos\gamma & \tan\vartheta\sin\gamma \end{bmatrix},$$

$$f_3(x_2, x_3) = \begin{bmatrix} \dfrac{\left(m_x^{\alpha}\alpha + m_x^{\beta}\beta\right)QSL}{J_x} + \dfrac{J_y - J_z}{J_x}\omega_y\omega_z \\ \dfrac{m_y^{\beta}\beta QSL}{J_y} + \dfrac{J_z - J_x}{J_y}\omega_z\omega_x \\ \dfrac{m_z^{\alpha}\alpha QSL}{J_z} + \dfrac{J_x - J_y}{J_z}\omega_x\omega_y \end{bmatrix},$$

$$g_3 = \begin{bmatrix} \dfrac{m_x^{\delta_x}QSL}{J_x} & 0 & 0 \\ 0 & \dfrac{m_y^{\delta_y}QSL}{J_y} & 0 \\ 0 & 0 & \dfrac{m_z^{\delta_z}QSL}{J_z} \end{bmatrix},$$

$$d_2(t) = \begin{bmatrix} \Delta_{\alpha} \\ \Delta_{\beta} \\ \Delta_{\gamma} \end{bmatrix},$$

$$d_3(t) = \begin{bmatrix} \Delta_{\omega_x} \\ \Delta_{\omega_y} \\ \Delta_{\omega_z} \end{bmatrix}. \tag{10}$$

Due to the existence of factors such as large target maneuvers, unsatisfactory initial states in the shift phase of middle and final guidance, external interference, and system uncertainty, the state variables such as α, β, γ, ω_x, ω_y, and ω_z may exceed the allowable ranges, which will worsen the dynamic quality of the system, affect the control performance, and even lead to control divergence.

In this paper, the research goal is to design an IGC algorithm that makes the missile system state variables and rudder angles not exceed the allowed ranges and the LOS angles and angular rates converge in fixed-time.

2.2. Preliminaries. The following definitions and lemmas are given for analysis convenience.

Definition 1. Define $y = [y_1, y_2, \cdots, y_n]^T$, sgn $(\cdot)$ is sign function and sgn $(0) = 0$, $\text{sgn}^a(y) = |y|^a \text{ sgn } (y)$, and $|y|^a = \text{diag } (|y_1|^a, \cdots, |y_n|^a)$.

Definition 2. For a nonlinear system $\dot{x}(t) = f(x(t))$, $x(0) = x_0$, if there is a moment $T_{\max} > 0$, for any $x_0 \in R$, $t > T_{\max}$, satisfying $x(t) = 0$, the system is fixed-time stable.

Lemma 3 (see [22, 23]). *For the system $\dot{y} = -a_1 \text{ sgn}^{b_1}(y) - a_2 \text{ sgn}^{b_2}(y)$, and $a_1 > 0$, $a_2 > 0$, $0 < b_1 < 1$, and $b_2 > 1$, then the system is stable in fixed-time and the convergence time satisfies*

$$T_1 < \frac{1}{a_1(1 - b_1)} + \frac{1}{a_2(b_2 - 1)}. \tag{11}$$

In addition, if the system has a small disturbance, that is $\dot{y} = -a_1 \text{ sgn}^{b_1}(y) - a_2 \text{ sgn}^{b_2}(y) + \varsigma$, ς is a small positive number, then the system can converge to the neighborhood of the origin $\Omega = \{|y| \le 2\vartheta | a_1\vartheta^{b_1} + a_2 b_1 \vartheta^{b_2} = \varsigma\}$ in fixed-time, and the convergence time satisfies

$$T_2 < \frac{1}{a_1\left(2^{b_1} - 1\right)(1 - b_1)} + \frac{1}{a_2(b_2 - 1)}. \tag{12}$$

Lemma 4 (see [24]). *Assuming that the Lyapunov function $V(x)$ satisfies $\dot{V}(\mathbf{x}) \le -a_1 V^{b_1}(\mathbf{x}) - a_2 V^{b_2}(\mathbf{x})$, and $a_1 > 0$, $a_2 > 0$, $0 < b_1 < 1$, and $b_2 > 1$, then the system is stable in fixed-time and the convergence time satisfies*

$$T_3 < \frac{1}{a_1(1 - b_1)} + \frac{1}{a_2(b_2 - 1)}. \tag{13}$$

Lemma 5 (see [25]). *For any real number x_i, $i = 1, 2, \cdots, n$, there are real numbers $0 < a < 1$ and $b > 1$, such that the following equations are true*

$$\left(\sum_{i=1}^{n}|x_i|\right)^a \le \sum_{i=1}^{n}|x_i|^a, \qquad \left(\sum_{i=1}^{n}|x_i|\right)^b \le n^{b-1}\sum_{i=1}^{n}|x_i|^b. \tag{14}$$

According to Lemma 5, the following equations hold

$$\begin{cases} x^T \operatorname{sgn}^a(x) = \sum_{i=1}^{n} \left|x_i^2\right|^{(a+1)/2} \geq \left(\sum_{i=1}^{n} \left|x_i^2\right|\right)^{(a+1)/2} = \|\mathbf{x}\|^{a+1}, \\ x^T \operatorname{sgn}^b(x) \geq n^{1-(b+1)/2} \left(\sum_{i=1}^{n} \left|x_i^2\right|\right)^{(b+1)/2} = n^{(1-b)/2} \|\mathbf{x}\|^{b+1}. \end{cases} \tag{15}$$

3. IGC Design and Stability Analysis

The IGC model (9) established in this paper is a strict-feedback nonlinear system with uncertainty, so the backstepping control design method is used to accomplish the IGC scheme. The backstepping control is improved based on fixed-time stability theory to let the system states fixed-time convergence. A second-order instruction filter is introduced into backstepping control to overcome "differential expansion." On the one hand, the derivatives of virtual control quantities are realized through integration, and the noise influence on the system is effectively reduced. On the other hand, the system states and actual control instructions are constrained to ensure that they do not exceed the allowable ranges.

3.1. Novel IGC Law Design. For the missile attacking the target accurately with desired terminal LOS angle, that is, the system states x_0 and x_1 fixed-time converge to zero, based on Lemma 5 and piecewise sliding mode surface idea, a fixed-time convergence sliding mode is designed as

$$s_1 = x_1 + k_1 \operatorname{sgn}^{a_1}(x_0) + k_2 \boldsymbol{\varphi}(x_0), \tag{16}$$

where $\boldsymbol{\varphi}(x_0) = [\varphi(x_{01}), \varphi(x_{02})]^{\mathrm{T}}$,

$$\varphi(x_{0i}) = \begin{cases} x_{0i}^{a_2}, |x_{0i}| \geq \delta, \\ \lambda_1 x_{0i} + \lambda_2 x_{1i}^3, |x_{1i}| < \delta, \end{cases} \tag{17}$$

where $a_1 > 1$, $0 < a_2 = p_1/p_2 < 1$, $k_i = \operatorname{diag}(k_{i1}, k_{i2})$ is the positive definite matrix to be designed, $i = 1, 2$, $\delta > 0$, p_1, and p_2 are odd numbers, $\lambda_1 = (3 - a_2)\delta^{\alpha_2 - 1}/2$, and $\lambda_2 = (a_2 - 1)\delta^{\alpha_2 - 3}/2$.

The time derivative of (16) is given by

$$\dot{s}_1 = \dot{x}_1 + k_1 a_1 |x_0|^{a_1 - 1} x_1 + k_2 \varphi'(x_0) x_1, \tag{18}$$

with

$$\varphi'(x_{0i}) = \begin{cases} a_2 |x_{0i}|^{a_2 - 1}, |x_{0i}| \geq \delta, \\ \lambda_1 + 3\lambda_2 x_{0i}^2, |x_{0i}| < \delta, \\ i = 1, 2. \end{cases} \tag{19}$$

Based on fixed-time stability theory, backstepping control, and the above sliding mode surface, the design process of the novel IGC scheme with multiple constraints are as follows:

Step 1. Define the tracking error as

$$s_1 = x_1 + k_1 \operatorname{sgn}^{a_1}(x_0) + k_2 \varphi(x_0). \tag{20}$$

The time derivative of s_1 is given by

$$\begin{aligned} \dot{s}_1 &= \dot{x}_1 + k_1 a_1 |x_0|^{a_1 - 1} x_1 + k_2 \varphi'(x_0) x_1 \\ &= f_1 + g_1 x_2^{\#} + d_1 + k_1 a_1 |x_0|^{a_1 - 1} x_1 + k_2 \varphi'(x_0) x_1. \end{aligned} \tag{21}$$

Design the virtual control law of $x_2^{\#}$ as

$$\begin{aligned} x_{2c}^{\#} = -g_1^{-1} \Big[& f_1 + \widehat{d}_1 + k_1 a_1 |x_0|^{a_1 - 1} x_1 + k_2 \varphi'(x_0) x_1 \\ & + k_3 \operatorname{sgn}^{b_1}(s_1) + k_4 \operatorname{sgn}^{b_2}(s_1) + \nu_1 \Big], \end{aligned} \tag{22}$$

where $b_1 > 1$, $0 < b_2 = p_3/p_4 < 1$, p_3 and p_4 are odd numbers, k_3 and k_4 are positive definite diagonal matrixes to be designed, and ν_1 is filter tracking error compensation, which is used to compensate the influence of instruction filter on virtual control law, and its definition will be given later. $\widehat{d}_1$ is the estimation of d_1. Here, the observer proposed in [26] is used to estimate the disturbances, and the specific expression is

$$\begin{cases} \dot{\hat{x}}_1 = f_1(x_1) + g_1(x_1) x_2^{\#} + \widehat{d}_1, \\ \widehat{d}_1 = \lambda_{11} \operatorname{sgn}^{\gamma_1}(\tilde{x}_1) + \lambda_{12} \operatorname{sgn}^{\gamma_2}(\tilde{x}_1) + \lambda_{13} \int_0^t \operatorname{sgn}(\tilde{x}_1(\tau)) \mathrm{d}\tau, \end{cases} \tag{23}$$

where $\lambda_{1i} > 0$ $(i = 1, 2, 3)$, $\tilde{x}_1 = x_1 - \hat{x}_1$, and $\hat{x}_1$ is the estimation of x_1.

In order to avoid "differential expansion" and considering the limitation of virtual control variables, a new virtual control law was introduced by referring to the dynamic surface design method. $x_{2d}^{\#}$ and its derivative $\dot{x}_{2d}^{\#}$ are obtained by passing through a second-order instruction filter. The state space expression of the filter is

$$\begin{bmatrix} \dot{q}_1 \\ \dot{q}_2 \end{bmatrix} = \begin{bmatrix} q_2 \\ 2\zeta\omega_n \left\{ \frac{\omega_n^2}{2\zeta\omega_n} [S_M(x_c) - q_1] - q_2 \right\} \end{bmatrix}, \tag{24}$$

$$\begin{bmatrix} x_d \\ \dot{x}_d \end{bmatrix} = \begin{bmatrix} q_1 \\ q_2 \end{bmatrix}, \tag{25}$$

where $S_M(\cdot)$ is the saturation function, which is defined as

$$S_M(x) = \begin{cases} M \operatorname{sgn}(x), |x| \geq M, \\ x, |x| < M. \end{cases} \tag{26}$$

It can be seen from (24) and (25) that the calculation of $\dot{x}_d$ does not need a differentiator, thus avoiding the problem of "differential expansion." If x_c is bounded, then both x_d

and $\dot{x}_d$ are continuously bounded. By selecting a larger natural frequency ω_n, $|x_d - x_c|$ can be made small. However, if it is too large, it will bring high frequency noise to the system, so compromise should be considered when selecting parameters.

The expression of v_1 is

$$\dot{\mathbf{v}}_1 = \begin{cases} -l_1\left(\operatorname{sgn}^{b_1}(v_1) + \operatorname{sgn}^{b_2}(v_1)\right) + \dfrac{v_1 s_1^{\mathrm{T}} g_1\left(x_{2d}^{\#} - x_{2c}^{\#}\right)}{\|v_1\|^2}, \|v_1\| > \mu_1, \\ 0, \|v_1\| \le \mu_1, \end{cases} \tag{27}$$

where l_1 is the positive definite diagonal matrix to be designed and μ_1 is a smaller positive number.

Step 2. Define the tracking error as $s_2 = x_2 - x_{2d}$ and $x_{2d} = [x_{2d}^{\#}; 0]$. The time derivative of s_2 is given by

$$\dot{s}_2 = \dot{x}_2 - \dot{x}_{2d} = f_2 + g_2 x_3 + d_2 - \dot{x}_{2d}. \tag{28}$$

The virtual control quantity of x_3 is designed as

$$x_{3c} = -g_2^{-1}\left[f_2 + \dot{x}_{2d} + \hat{d}_2 + k_5 \operatorname{sgn}^{b_1}(s_2) + k_6 \operatorname{sgn}^{b_2}(s_2) + v_2 + \boldsymbol{\chi}\right], \tag{29}$$

where k_5 and k_6 are positive definite diagonal matrixes to be designed, $\boldsymbol{\chi} = [g_1^{\mathrm{T}} s_1\ 0]^{\mathrm{T}}$.

Let x_{3c} pass through the second-order filter to get x_{3d} and $\dot{x}_{3d}$. The expression of v_2 is

$$\dot{\mathbf{v}}_2 = \begin{cases} -l_2\left(\operatorname{sgn}^{b_1}(v_2) + \operatorname{sgn}^{b_2}(v_2)\right) + \dfrac{v_2 s_2^{\mathrm{T}} g_2(x_{3d} - x_{3c})}{\|v_2\|^2}, \|v_2\| > \mu_2, \\ 0, \|v_2\| \le \mu_2. \end{cases} \tag{30}$$

Step 3. The tracking error is defined as $s_3 = x_3 - x_{3d}$. The time derivative of $\mathbf{s}_3$ is given by

$$\dot{s}_3 = \dot{x}_3 - \dot{x}_{3d} = f_3 + g_3 u + d_3 - \dot{x}_{3d}. \tag{31}$$

The virtual control law of u is designed as

$$u_c = -g_3^{-1}\left[f_3 + \dot{x}_{3d} + \hat{d}_3 + k_7 \operatorname{sgn}^{b_1}(s_2) + k_8 \operatorname{sgn}^{b_2}(s_2) + v_3 + g_2^{\mathrm{T}} s_2\right]. \tag{32}$$

Let u_c pass through the second-order filter to get the actual IGC law u. The expression of v_3 is

$$\dot{\mathbf{v}}_3 = \begin{cases} -l_3\left(\operatorname{sgn}^{b_1}(v_3) + \operatorname{sgn}^{b_2}(v_3)\right) - \dfrac{v_3 s_3^{\mathrm{T}} g_3(u - u_c)}{\|v_3\|^2}, \|v_3\| > \mu_3, \\ 0, \|v_3\| \le \mu_3. \end{cases} \tag{33}$$

The IGC algorithm structure is illustrated in Figure 2.

3.2. Stability Analysis

Theorem 6. *For the system (9), the proposed novel IGC law from (20) to (33) can guarantee that the system states x_0 and x_1 converge to the origin neighborhood in fixed-time, and the closed-loop IGC system is stable in spite of disturbances.*

Proof. From (21) to (32), we can obtain

$$\begin{aligned} \dot{s}_1 &= f_1 + g_1\left(s_2^{\#} + x_{2d}^{\#} - x_{2c}^{\#} + x_{2c}^{\#}\right) + d_1 \\ &\quad + k_1 a_1 |x_0|^{a_1 - 1} x_1 + k_2 \varphi'(x_0) x_1 \\ &= g_1\left(s_2^{\#} + x_{2d}^{\#} - x_{2c}^{\#}\right) - k_3 \operatorname{sgn}^{b_1}(s_1) \\ &\quad - k_4 \operatorname{sgn}^{b_2}(s_1) - v_1 + \tilde{d}_1, \end{aligned}$$

$$\begin{aligned} \dot{s}_2 &= f_2 + g_2(s_3 + x_{3d} - x_{3c} + x_{3c}) + d_2 - \dot{x}_{2d} \\ &= g_2(s_3 + x_{3d} - x_{3c}) - k_5 \operatorname{sgn}^{b_1}(s_2) \\ &\quad - k_6 \operatorname{sgn}^{b_2}(s_2) - v_2 - \boldsymbol{\chi} + \tilde{d}_2, \end{aligned}$$

$$\begin{aligned} \dot{s}_3 &= f_3 + g_3(u - u_c + u_c) + d_3 - \dot{x}_{3d} \\ &= g_3(u - u_c) - g_2^{\mathrm{T}} s_2 - k_7 \operatorname{sgn}^{b_1}(s_3) \\ &\quad - k_8 \operatorname{sgn}^{b_2}(s_3) - v_3 + \tilde{d}_3, \end{aligned} \tag{34}$$

where $\tilde{d}_i = d_i - \hat{d}_i (i = 1, 2, 3)$ and $s_2^{\#} = [s_{21}\ s_{22}]^{\mathrm{T}}$.

Construct the Lyapunov function

$$V = \frac{1}{2}\sum_{i=1}^{3}\left(s_i^{\mathrm{T}} s_i + v_i^{\mathrm{T}} v_i\right). \tag{35}$$

The time derivative of V is obtained as

$$\begin{aligned} \dot{V} &= \sum_{i=1}^{3}\left(s_i^{\mathrm{T}} \dot{s}_i + v_i^{\mathrm{T}} v_i\right) \\ &= s_1^{\mathrm{T}}\left[g_1\left(s_2^{\#} + x_{2d}^{\#} - x_{2c}^{\#}\right) + \tilde{d}_1 - k_3 \operatorname{sgn}^{b_1}(s_1) - k_4 \operatorname{sgn}^{b_2}(s_1) - v_1\right] \\ &\quad + s_2^{\mathrm{T}}\left[g_2(s_3 + x_{3d} - x_{3c}) + \tilde{d}_2 - k_5 \operatorname{sgn}^{b_1}(s_2) - k_6 \operatorname{sgn}^{b_2}(s_2) - v_2 - \boldsymbol{\chi}\right] \\ &\quad + s_3^{\mathrm{T}}\left[g_3(u - u_c) + \tilde{d}_3 - k_7 \operatorname{sgn}^{b_1}(s_3) - k_8 \operatorname{sgn}^{b_2}(s_3) - v_3 - g_2^{\mathrm{T}} s_2\right] \\ &\quad - v_1^{\mathrm{T}} l_1\left(\operatorname{sgn}^{b_1}(v_1) + \operatorname{sgn}^{b_2}(v_1)\right) - s_1^{\mathrm{T}} g_1\left(x_{2d}^{\#} - x_{2c}^{\#}\right) \\ &\quad - v_2^{\mathrm{T}} l_2\left(\operatorname{sgn}^{b_1}(v_2) + \operatorname{sgn}^{b_2}(v_2)\right) - s_2^{\mathrm{T}} g_2(x_{3d} - x_{3c}) \\ &\quad - v_3^{\mathrm{T}} l_3\left(\operatorname{sgn}^{b_1}(v_3) + \operatorname{sgn}^{b_2}(v_3)\right) - s_3^{\mathrm{T}} g_3(u - u_c) \\ &= s_1^{\mathrm{T}}\tilde{d}_1 - s_1^{\mathrm{T}} k_3 \operatorname{sgn}^{b_1}(s_1) - s_1^{\mathrm{T}} k_4 \operatorname{sgn}^{b_2}(s_1) - s_1^{\mathrm{T}} v_1 + s_2^{\mathrm{T}}\tilde{d}_2 \\ &\quad - s_2^{\mathrm{T}} k_5 \operatorname{sgn}^{b_1}(s_2) - s_2^{\mathrm{T}} k_6 \operatorname{sgn}^{b_2}(s_2) - s_2^{\mathrm{T}} v_2 + s_3^{\mathrm{T}}\tilde{d}_3 - s_3^{\mathrm{T}} k_7 \operatorname{sgn}^{b_1}(s_3) \\ &\quad - s_3^{\mathrm{T}} k_8 \operatorname{sgn}^{b_2}(s_3) - s_3^{\mathrm{T}} v_3 - v_1^{\mathrm{T}} l_1\left(\operatorname{sgn}^{b_1}(v_1) + \operatorname{sgn}^{b_2}(v_1)\right) \\ &\quad - v_2^{\mathrm{T}} l_2\left(\operatorname{sgn}^{b_1}(v_2) + \operatorname{sgn}^{b_2}(v_2)\right) - v_3^{\mathrm{T}} l_3\left(\operatorname{sgn}^{b_1}(v_3) + \operatorname{sgn}^{b_2}(v_3)\right). \end{aligned} \tag{36}$$

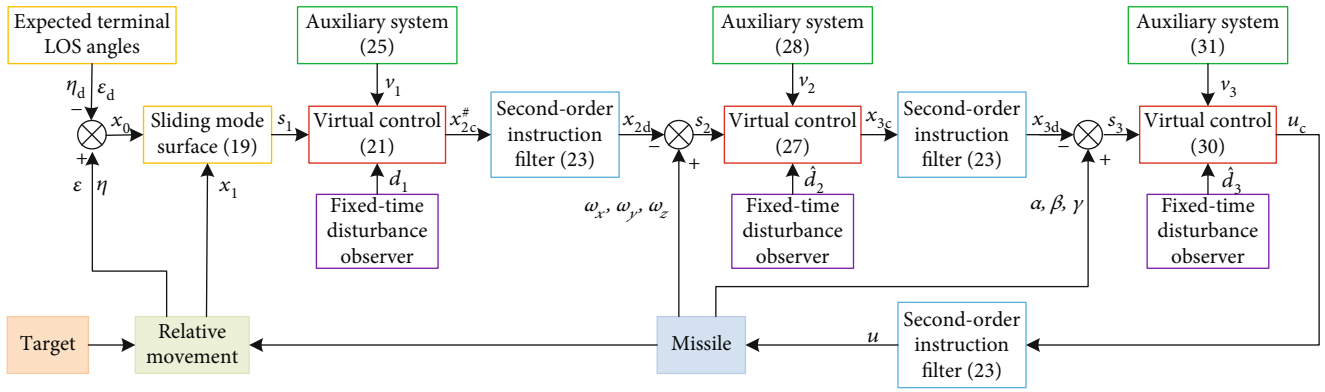

Figure 2: Multiple constraint fixed-time IGC algorithm structure.

Table 1: The initial condition for missile and target.

Symbol	Value	Symbol	Value	Symbol	Value
x_m	0 m	x_t	5000 m	α	8 deg
y_m	5000 m	y_t	1000 m	β	4 deg
z_m	0 m	z_t	2000 m	γ	8 deg
V_m	600 m/s	V_t	50 m/s	ω_x	20 deg/s
θ_m	15 deg	θ_t	0 deg	ω_y	-20 deg/s
ψ_m	-5 deg	ψ_t	0 deg	ω_z	-30 deg/s

Table 2: Missile dynamic parameters.

Symbol	Value	Symbol	Value	Symbol	Value
m	1200 kg	m_x^{α}	0.45	C_y^{α}	57.15
S	0.42 m^2	m_x^{β}	-0.38	C_y^{β}	-0.081
L	0.69 m	$m_x^{\delta_x}$	2.13	$C_y^{\delta_z}$	5.75
J_x	100 kg·m^2	m_y^{β}	-27.30	C_z^{α}	0.09
J_y	5800 kg·m^2	$m_y^{\delta_y}$	-26.60	C_z^{β}	-56.32
J_z	5700 kg·m^2	m_z^{α}	-28.15	$C_z^{\delta_y}$	-5.6
g	9.8 m/s^2	$m_z^{\delta_z}$	-27.90		

Table 3: Constraints of states and actuators.

Symbol	Range	Symbol	Range
α	[-10, 10] deg	ω_x, ω_z	[-40, 40] deg/s
β	[-5, 5] deg	ω_y	[-30, 30] deg/s
γ	[-10, 10] deg	δ_x, δ_y, δ_z	[-12, 12] deg

According to (15), it can be obtained as

$$\dot{V} \le -3^{(1-b_1)/2}\sum_{i=1}^{3}\left(\lambda_{\min}(k_{2i+1})\|s_i\|^{b_1+1} + \lambda_{\min}(l_i)\|v_i\|^{b_1+1}\right) - \sum_{i=1}^{3}\left(\lambda_{\min}(k_{2i+2})\|s_i\|^{b_2+1} + \lambda_{\min}(l_i)\|v_i\|^{b_2+1}\right) + \sum_{i=1}^{3}\left(s_i^{\mathrm{T}}\tilde{d}_i - s_i^{\mathrm{T}}v_i\right). \tag{37}$$

Based on the Young inequality, we can get

$$s_i^{\mathrm{T}}\tilde{d}_i \le \frac{1}{2}s_i^{\mathrm{T}}s_i + \frac{1}{2}\tilde{d}_i^{\mathrm{T}}\tilde{d}_i, \tag{38}$$

$$-s_i^{\mathrm{T}}v_i \le \frac{1}{2}s_i^{\mathrm{T}}s_i + \frac{1}{2}v_i^{\mathrm{T}}v_i. \tag{39}$$

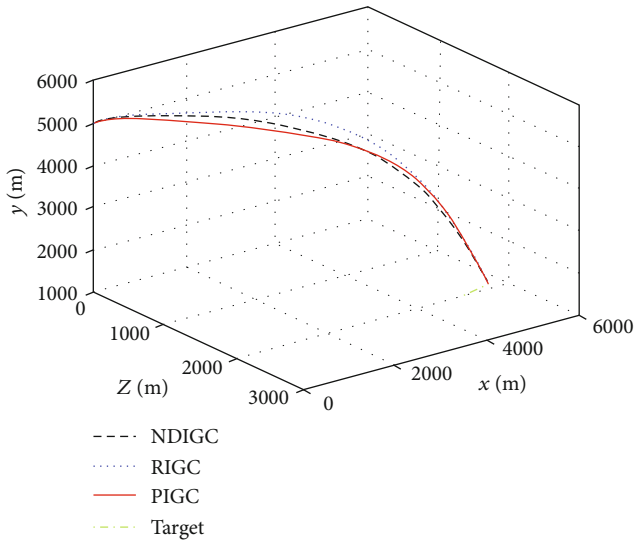

Figure 3: Trajectories of missile and target in case 1.

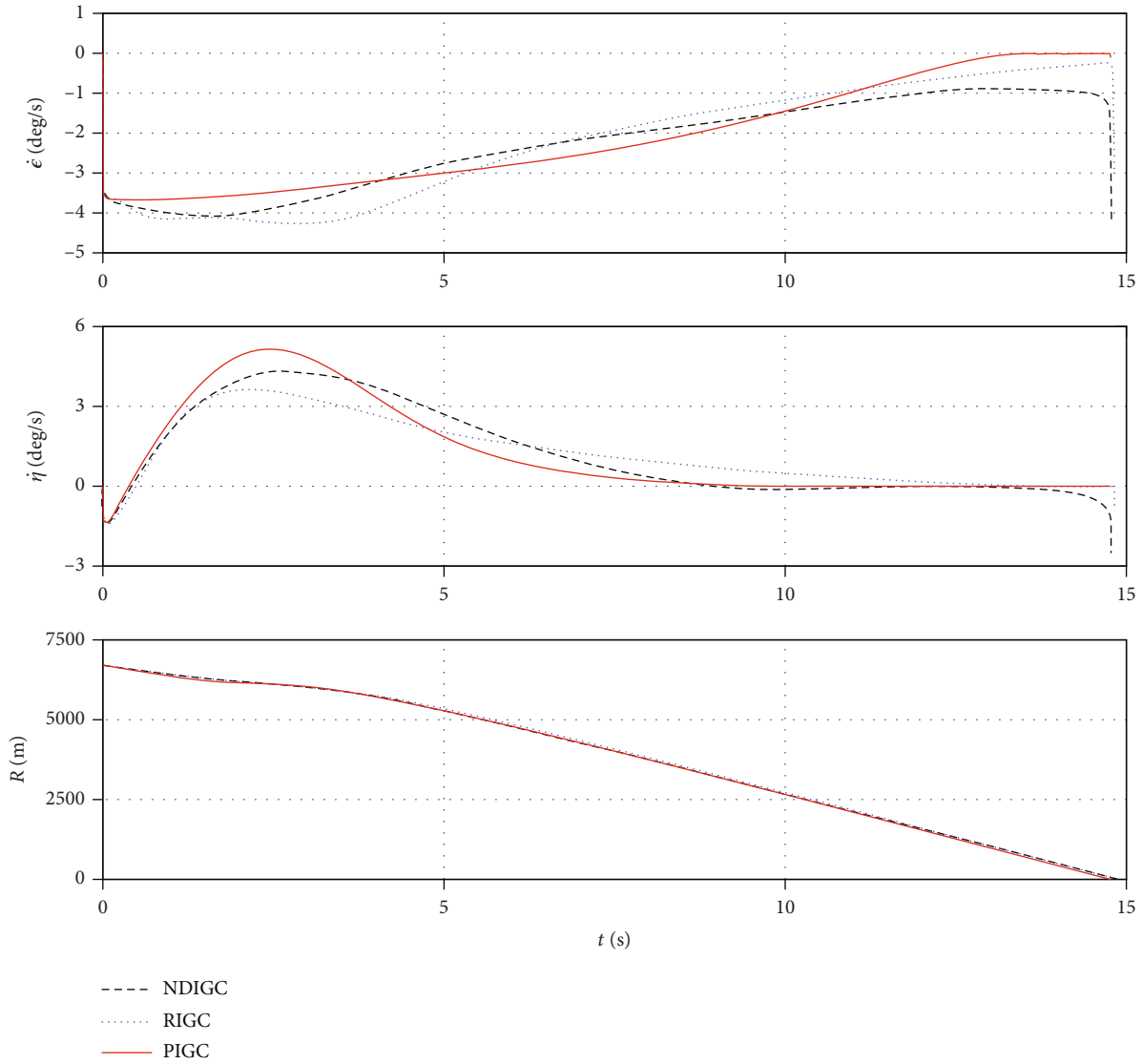

Figure 4: LOS angular rates and relative distances in case 1.

Table 4: Simulation results of three IGC laws.

IGC law	NDIGC	RIGC	PIGC
Intercept time (s)	14.87	14.91	14.77
Miss distance (m)	1.33	2.31	0.71
LOS elevation angle error (deg)	0.28	0.34	0.05
LOS azimuth angle error (deg)	0.12	0.21	0.04

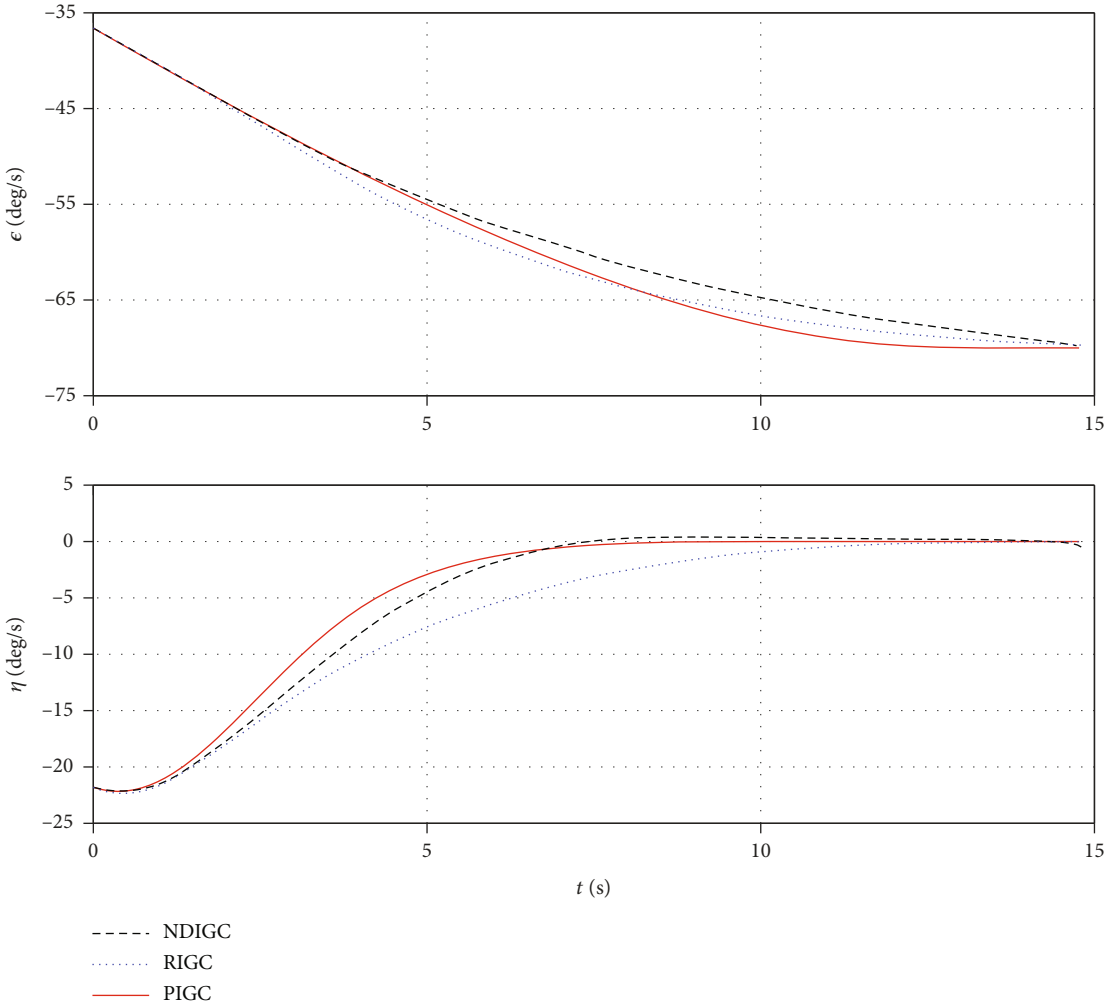

Figure 5: LOS elevation and azimuth angles in case 1.

Consider the following inequality:

$$p \le p^{m_1} + p^{m_2}, \tag{40}$$

where $p \ge 0$, $m_1 > 1$, and $0 < m_2 < 1$. Then, the following inequality holds

$$-n_1 p^{m_1} - n_2 p^{m_2} + n_3 p \le -(n_1 - n_3) p^{m_1} - (n_2 - n_3) p^{m_2}, \tag{41}$$

where $n_1 > 0$, $n_2 > 0$, and $n_3 > 0$.

Combining with (38), (39), and (41), equation (37) can be written as

$$\begin{aligned}\dot{V} \le & -3^{(1-b_1)/2} \sum_{i=1}^{3} \left[(\lambda_{\min}(k_{2i+1}) - 1) \|s_i\|^{b_1+1} + \left(\lambda_{\min}(l_i) - \frac{1}{2}\right) \|v_i\|^{b_1+1} \right] \\ & - \sum_{i=1}^{3} \left[(\lambda_{\min}(k_{2i+2}) - 1) \|s_i\|^{b_2+1} + \left(\lambda_{\min}(l_i) - \frac{1}{2}\right) \|v_i\|^{b_2+1} \right] \\ & + \frac{1}{2} \sum_{i=1}^{3} \tilde{d}_i^{\mathrm{T}} \tilde{d}_i. \end{aligned} \tag{42}$$

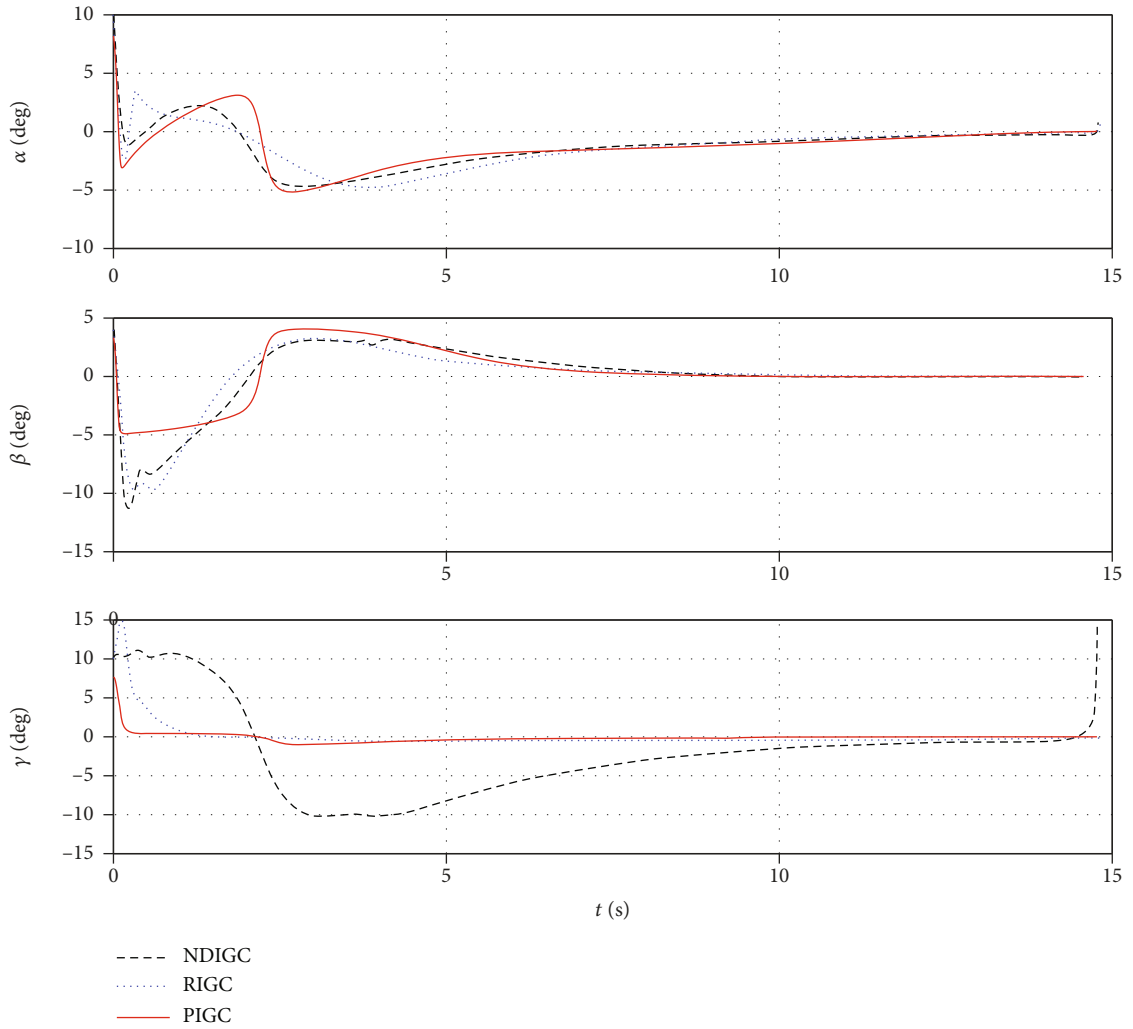

Figure 6: Attack, sideslip, and roll angles in case 1.

Select appropriate parameters satisfying

$$\begin{cases} \lambda_{\min}(k_{2i+1}) - 1 \geq 18^{(b_1-1)/2}k, \\ \lambda_{\min}(l_i) - \dfrac{1}{2} \geq 18^{(b_1-1)/2}k, \\ \lambda_{\min}(k_{2i+2}) - 1 \geq k, \\ \sigma = \dfrac{1}{2}\left(\tilde{d}_1^{\mathrm{T}}\tilde{d}_1 + \tilde{d}_2^{\mathrm{T}}\tilde{d}_2 + \tilde{d}_3^{\mathrm{T}}\tilde{d}_3\right), \\ i = 1, 2, 3, \end{cases} \tag{43}$$

where $k > 0$.

Then, equation (42) can be written as

$$\begin{aligned} V \leq & -6^{(b_1-1)/2}k\sum_{i=1}^{3}\left[\left(\|s_i\|^2\right)^{(b_1+1)/2} + \left(\|v_i\|^2\right)^{(b_1+1)/2}\right] \\ & - k\sum_{i=1}^{3}\left[\left(\|s_i\|^2\right)^{(b_2+1)/2} + \left(\|v_i\|^2\right)^{(b_2+1)/2}\right] + \sigma. \end{aligned} \tag{44}$$

By Lemma 5 and (44), one can obtain

$$\begin{aligned} \dot{V} \leq & -k\left(\sum_{i=1}^{3}\left(\|s_i\|^2 + \|v_i\|^2\right)\right)^{(b_1+1)/2} \\ & + \sigma - k\left(\sum_{i=1}^{3}\left(\|s_i\|^2 + \|v_i\|^2\right)\right)^{(b_2+1)/2} \\ = & -kV^{(b_1+1)/2} - kV^{(b_2+1)/2} + \sigma. \end{aligned} \tag{45}$$

Since $(b_1 + 1)/2 > 1$ and $1/2 < (b_2 + 1)/2 < 1$, according to Lemma 4, V can fixed-time converge to a small neighborhood as

$$\Omega_1 = \left\{V \leq 2\vartheta_1 \middle| k\vartheta_1^{(b_1+1)/2} + k\vartheta_1^{(b_2+1)/2} = \sigma\right\}. \tag{46}$$

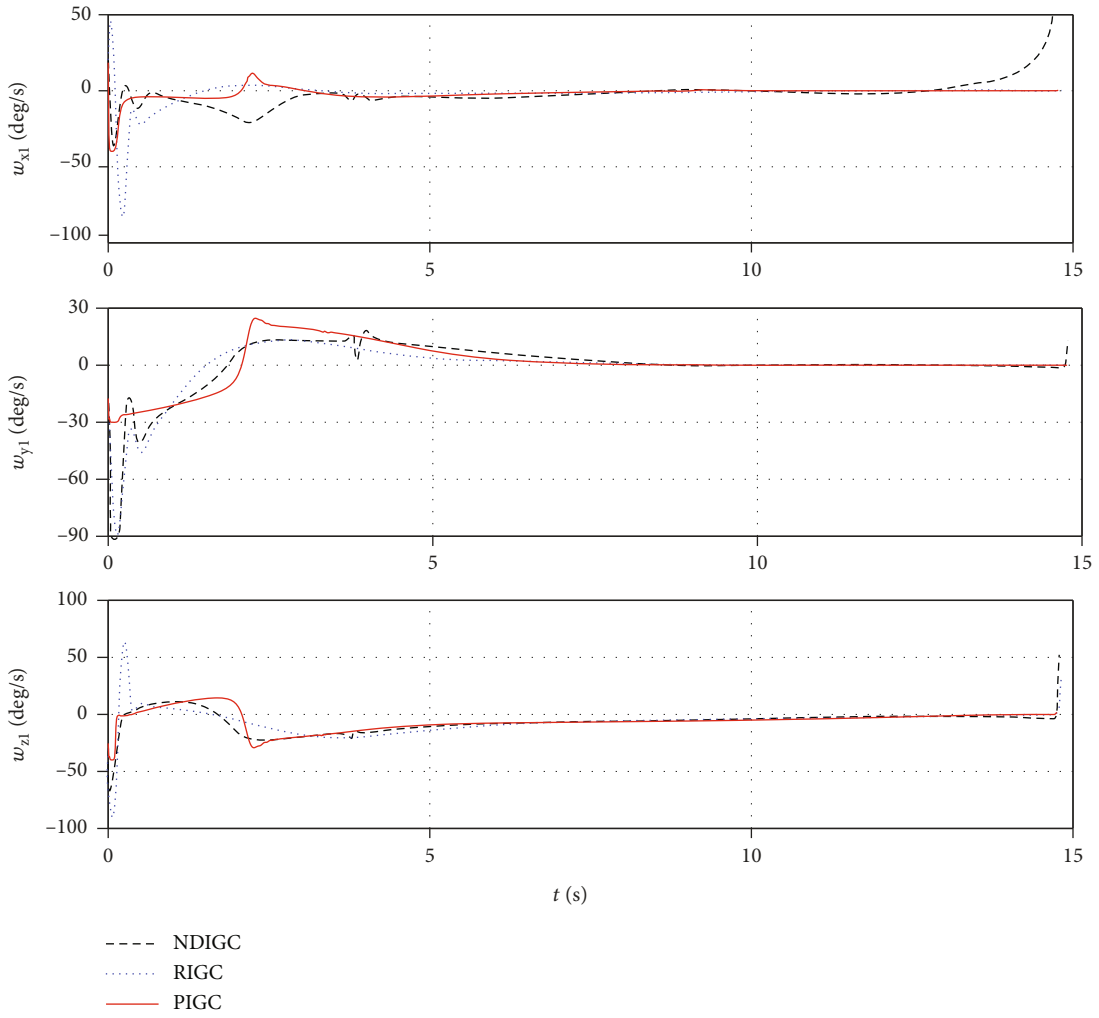

Figure 7: Roll, yaw, and pitch angular rates in case 1.

And the convergence time satisfies

$$t_1 < \frac{1}{k(b_1 - 1)} + \frac{1}{k\left(2^{(b_2+1)/2} - 1\right)(1 - b_2)}. \tag{47}$$

Combining with (46) and (35), s_1 can converge in fixed-time t_1 to the region $s_1 \le \sqrt{2\vartheta_1}$. Define $\Delta = \sqrt{2\vartheta_1}$, then $|s_{1i}| \le \Delta$, $i = 1, 2$. According to the region where the value of x_{0i} is located, the convergence region of x_{0i} and x_{1i} can be obtained as follows.

(a) When $|x_{0i}| > \delta$, it can be obtained from (16) that

$$\dot{x}_{0i} = -k_{1i}\,\mathrm{sgn}^{a_1}(x_{0i}) - k_{2i}\,\mathrm{sgn}^{a_2}(x_{0i}) + \phi_i, |\phi_i| \le \Delta \tag{48}$$

According to Lemma 4, x_{0i} can converge to the region $\Omega_{2i} = \{|x_{0i}| \le 2\vartheta_{2i}|k_{1i}\vartheta_{2i}^{a_1} + k_{2i}\vartheta_{2i}^{a_2} \le \Delta\}$, x_{1i} can converge to the region

$$|x_{1i}| \le k_{1i}|x_{0i}|^{a_1} + k_{2i}|x_{0i}|^{a_2} + |\phi_i| \le k_{1i}(2\vartheta_{2i})^{a_1} + k_{2i}(2\vartheta_{2i})^{a_2} + \Delta, \tag{49}$$

and convergence time satisfies

$$t_2 < \frac{1}{k_{1i}(a_1 - 1)} + \frac{1}{k_{2i}(2^{a_2} - 1)(1 - a_2)}. \tag{50}$$

(b) When $|x_{0i}| < \delta$, it can be obtained from (16) that

$$|x_{1i}| \le k_{1i}|x_{0i}|^{a_1} + k_{2i}\left|\lambda_1 x_{0i} + \lambda_2 x_{1i}^3\right| + |\phi_i| < k_{1i}\delta^{a_1} + k_{2i}\delta^{a_2} + \Delta \tag{51}$$

Based on the above analyses, x_{0i} and x_{1i} can converge to the neighborhood

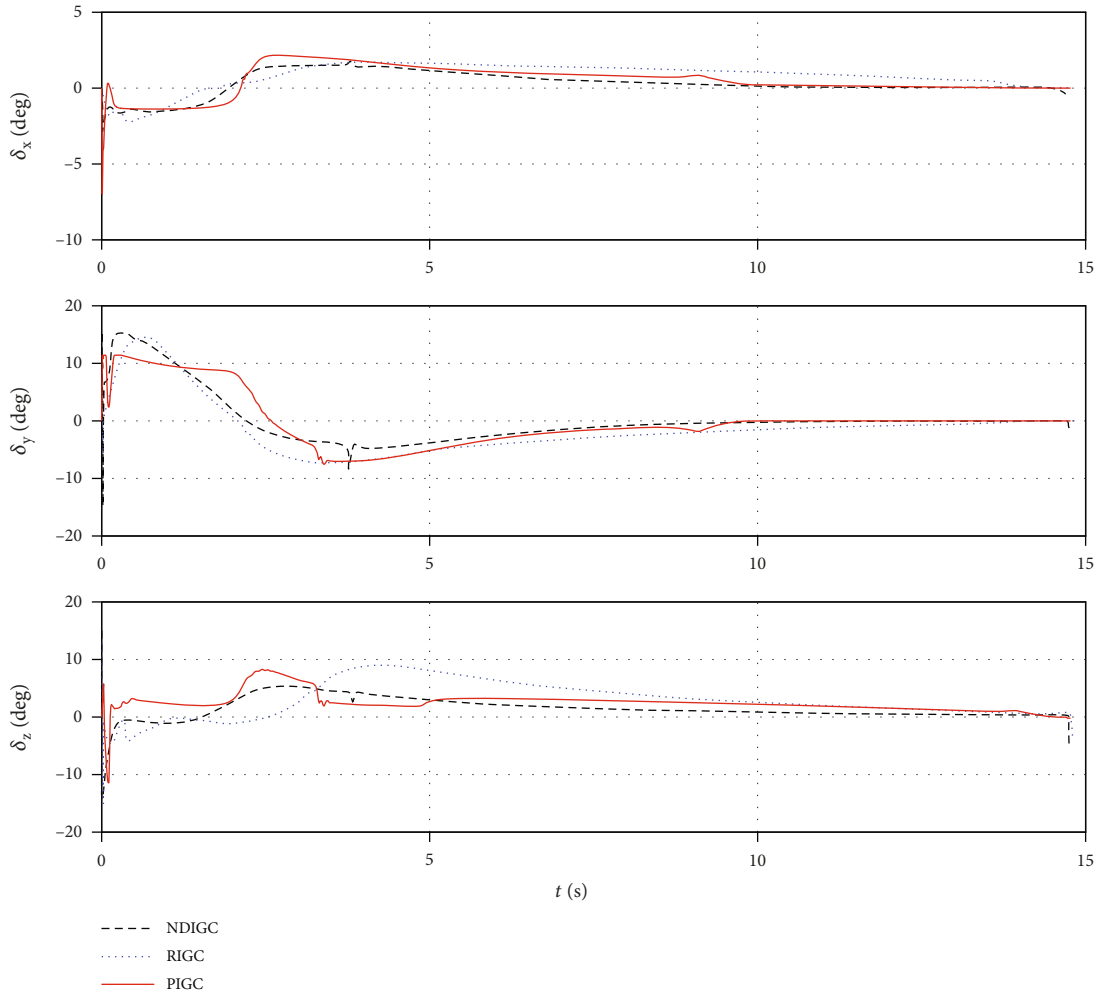

Figure 8: Roll, yaw, and pitch channel rudder angles in case 1.

$$\begin{cases} |x_{0i}| \le \kappa_i = \max\{2\vartheta_{2i}, \delta\}, k_{1i}{\vartheta_{2i}}^{a_1} + k_{2i}{\vartheta_{2i}}^{a_2} \le \Delta, \\ |x_{1i}| \le k_1{\kappa_i}^{a_1} + k_2{\kappa_i}^{a_2} + \Delta, \end{cases} \tag{52}$$

with fixed-time. In addition, we can get the convergence time which satisfies

$$t \le t_1 + t_2 < t_m = \frac{1}{k(b_1 - 1)} + \frac{1}{k\left(2^{(b_2+1)/2} - 1\right)(1 - b_2)} + \frac{1}{k_{1i}(a_1 - 1)} + \frac{1}{k_{2i}(2^{a_2} - 1)(1 - a_2)}. \tag{53}$$

It can be seen from (53) that the upper bound of convergence time t_m increases with the increase of k, k_{1i}, k_{2i}, a_1, and b_1 and increases with the decrease of a_2 and b_2. According to (43), k is related to the control parameter matrices $k_i (i = 3, 4, \cdots, 8)$ and $l_j (j = 1, 2, 3)$. Therefore, t_m only depends on the control parameters, independent of the system states.

Although the convergence speed of the IGC system states will increase as the parameters a_1, b_1, $k_i (i = 1, 2, \cdots, 8)$, and $l_j (j = 1, 2, 3)$ increase and decrease as the parameters a_2 and b_2 increase, excessive pursuit of convergence speed will produce large control instructions, requiring the missile to provide a large overload, and the missile available overload is limited, so compromise should be considered in parameter selection.

This completes the proof. □

4. Numerical Simulation Results and Analysis

The missile 6-DOF simulation is implemented to illustrate the performance of the proposed IGC (PIGC) design method. Table 1 shows the initial conditions of missile and target. Table 2 shows the missile dynamic parameters. The states and actuator constraints are described in Table 3. The lateral acceleration of the target is set as $a_{tz2} = 10 \sin(\pi t/2)$ m/s^2. Set the desired terminal LOS angles $\varepsilon_d = -70^\circ$ and $\eta_d = 0^\circ$.

There is an uncertainty $0.1\sin(0.2\pi t)$ for the missile inertia components and $0.2\sin(0.2\pi t)$ for aerodynamic coefficients. Set $\Delta\alpha = \Delta\beta = \Delta\gamma = 0.2 \sin(t)$rad/s and $\Delta\omega_x = \Delta\omega_y = \Delta\omega_z = \sin(t)$rad/s^2.

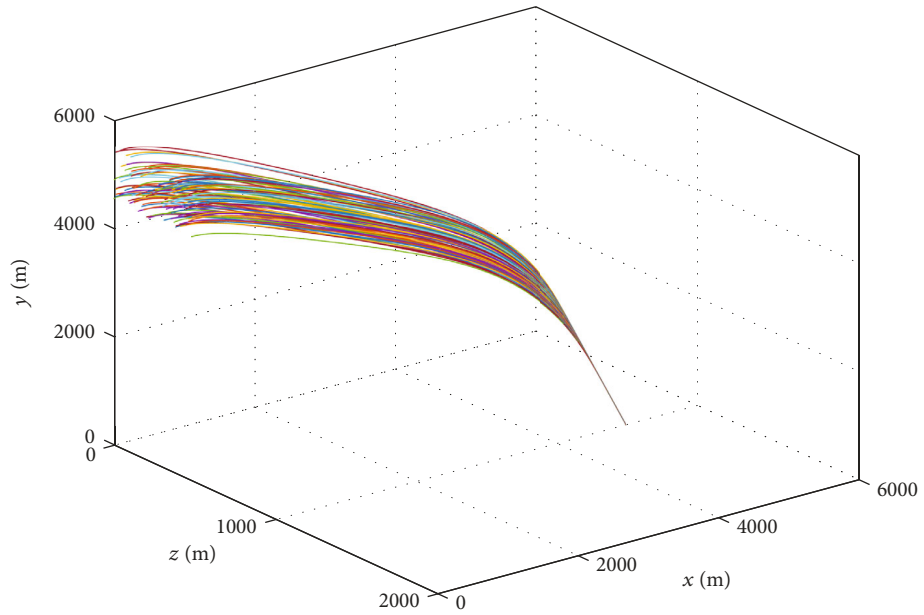

Figure 9: Trajectories of missile in case 2.

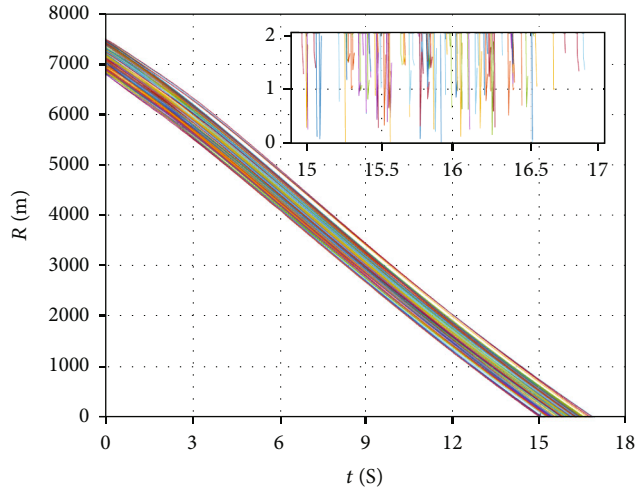

Figure 10: Relative distances of missile and target in case 2.

The design parameters for PIGC are set as $k_1 = \text{diag}(0.6, 1)$, $k_2 = \text{diag}(1, 1)$, $a_1 = 3$, $a_2 = 3/5$, $b_1 = 2$, $b_2 = 0.5$, $\mu_1 = \mu_2 = \mu_3 = 0.01$, $\delta = 0.01$, $k_3 = k_4 = \text{diag}(3, 4)$, $k_5 = k_6 = \text{diag}(8, 12, 12)$, $k_7 = k_8 = \text{diag}(20, 10, 10)$, $\boldsymbol{\zeta} = \text{diag}(0.6, 0.7, 0.6)$, $\boldsymbol{\omega}_n = \text{diag}(10, 20, 10)$, $l_1 = \text{diag}(3, 2, 5)$, $l_2 = \text{diag}(10, 8, 3)$, and $l_3 = \text{diag}(10, 10, 5)$. According to (53), it can be calculated that $t_m \approx 13.44$ s.

4.1. Case 1: Comparison Simulation with Existing Methods. The robust IGC design method (RIGC) proposed in [12] and the new dynamic surface control based IGC design method (NDIGC) proposed in [15] are introduced for comparative simulation analysis.

Missile and target trajectories, LOS angular rates, and relative distances are shown in Figures 3 and 4. The missile trajectories are relatively smooth under the three IGC laws. PIGC can make the LOS angular rates converge stably to near zero within fixed-time t_m and has a significant advantage in zeroing angular rates, thus leading to a small miss distance (see Table 4).

LOS angles are presented in Figure 5. It can be seen that the LOS angles can gradually converge to the expected value under the three IGC laws. The LOS angles of PIGC converge fastest. RIGC adopts sliding mode control to suppress disturbances such as model uncertainty and target maneuver. When there are large model uncertainties and disturbances, the convergence performance of RIGC is greatly affected. NDIGC selects linear sliding mode surface, which can only ensure the states convergent asymptotically. Therefore, PIGC is superior in terms of angle constraints and convergence.

The attack angles, sideslip angles, and roll angles curves are given in Figure 6. The three Euler angular rates are

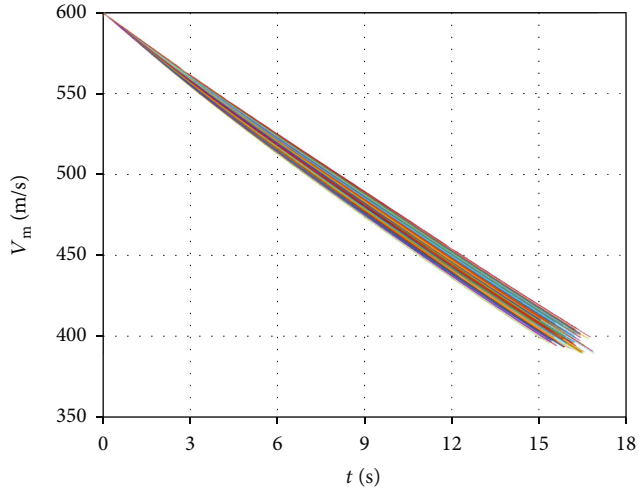

Figure 11: Missile velocities in case 2.

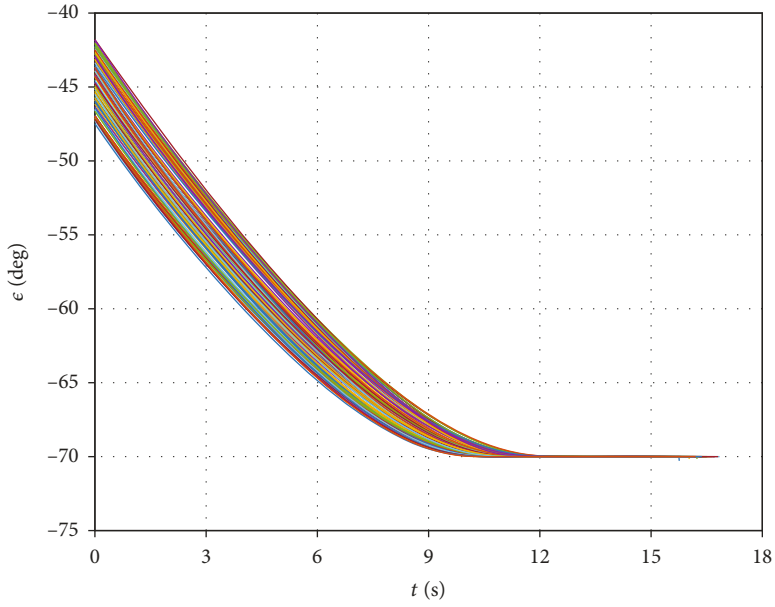

Figure 12: LOS elevation angles in case 2.

presented in Figure 7. The angles and angular rates can converge to near zero under three IGC algorithms. Compared with PIGC scheme, larger attack angle, sideslip angle, and roll angle result in larger pitch, yaw, and roll angular rates under RIGC and NDIGC. Moreover, the PCIGC can ensure that the system states do not exceed the constraint ranges.

The rudder angle curves are shown in Figure 8. Compared with RIGC, NDIGC and PIGC can restrict the rudder angles within the constraints. PIGC, in particular, can ensure that the rudder angles converge steadily to near zero in finite-time.

The simulation results in Figures 3, 5, and 6 seem divergent at the intercept time. This is because the relative motions of the missile and target change dramatically at the end, so the LOS angular rate changes dramatically and diverges at the last moment of the simulation. At the same time, as the system state constraints such as attack angle are not considered and corresponding virtual control instructions are not restricted, system states of RIGC and NDIGC cannot converge stably and diverge at the end of simulation.

Table 4 shows the simulation results of three IGC laws in terms of intercept times, miss distances, and LOS angle errors. It can be seen that PIGC has the smallest intercept time, miss distance, and angle errors. PIGC can impact the target accurately with shorter time, smaller miss distance, and higher angle constraint accuracy.

From the simulation results, it can be concluded that PIGC can effectively solve terminal angle constraints, state constraints, and control constraints and has fixed-time convergence, which is superior to NDIGC and RIGC.

4.2. Case 2: Monte Carlo Simulation. In this case, a missile intercepts a ground target. In case 1, it is assumed that

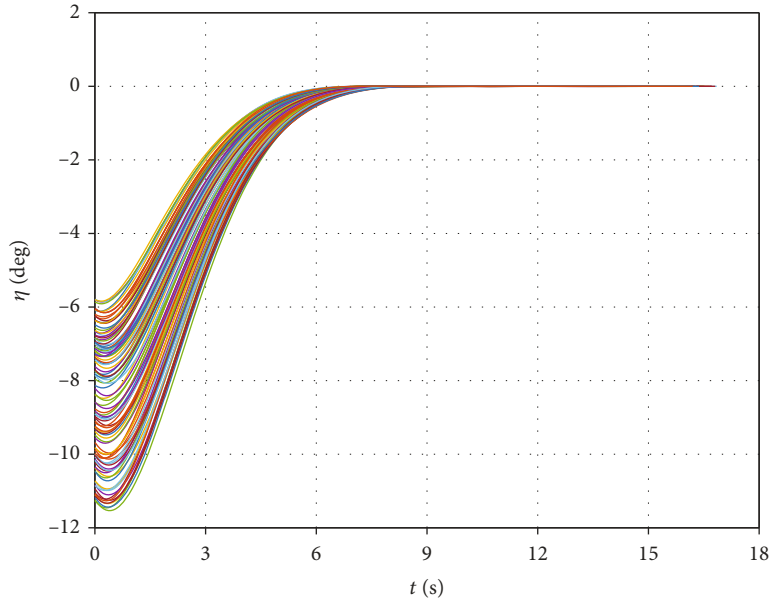

Figure 13: LOS azimuth angles in case 2.

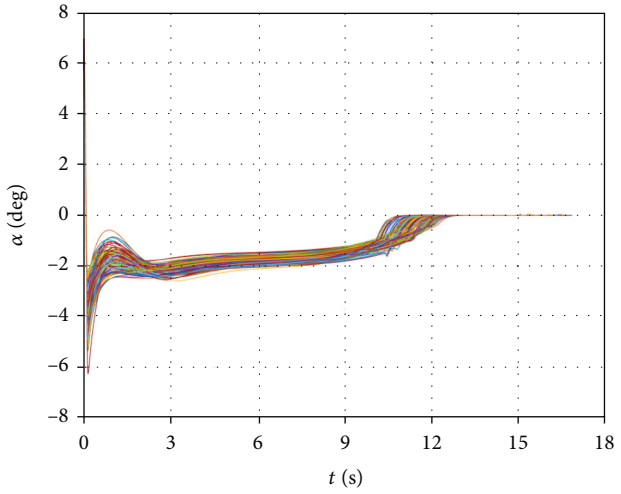

Figure 14: Attack angles in case 2.

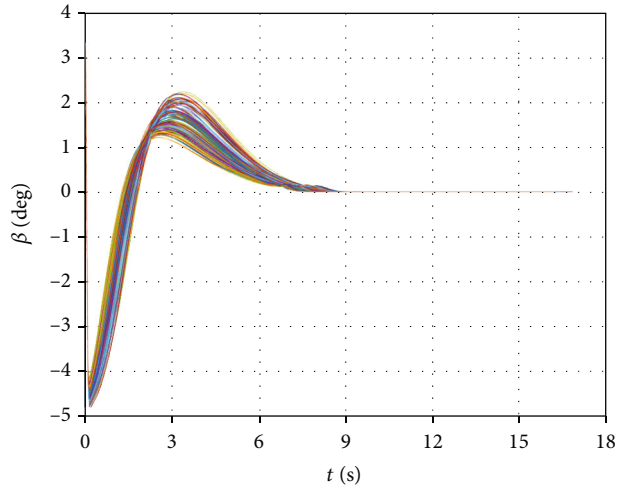

Figure 15: Sideslip angles in case 2.

the missile velocity is constant. But in a real scenario, the missile's speed would certainly change because of aerodynamic drag and gravity. Therefore, in order to be closer to engineering practice, the simulation under time-varying missile velocity will be considered in this case. At the same time, In order to further verify the robustness of PIGC algorithm, Monte Carlo simulation was carried out with 100 simulation times. Simulation conditions are as follows:

(1) The aerodynamic coefficients vary from -10% to +10% of the nominal value and follow normal distribution

(2) The mass and moment of inertia vary from -10% to +10% of the nominal value and follow normal distribution

(3) The initial position coordinates y_m and z_m of the missile vary randomly between 4500 m~5500 m and 0 m~500 m, respectively, subjected to normal distribution. The target position is (5000 m, 0 m, 1000 m)

(4) The missile initial fight path angle θ_m and heading angle ψ_{Vm} vary randomly between 0 deg~10 deg and -5 deg~0 deg, respectively, subjected to normal distribution

(5) The mathematical expression of aerodynamic resistance is

$$X = \left(C_{x0} + C_x^{\alpha}|\alpha| + C_x^{\beta}|\beta| + C_x^{\delta_x}|\delta_x| + C_x^{\delta_y}|\delta_y| + C_x^{\delta_z}|\delta_z|\right) Qs \tag{54}$$

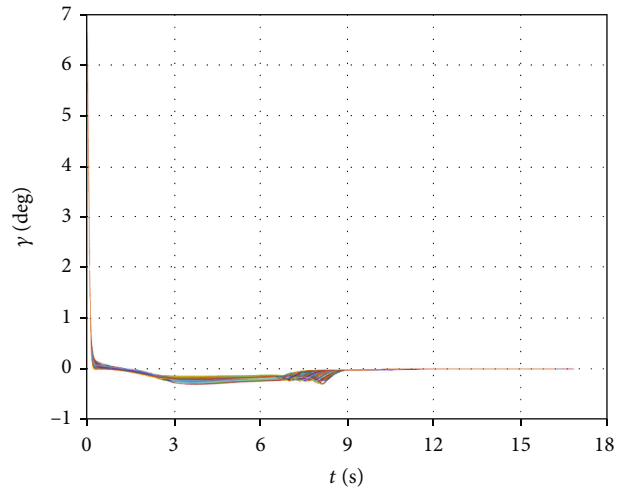

Figure 16: Roll angles in case 2.

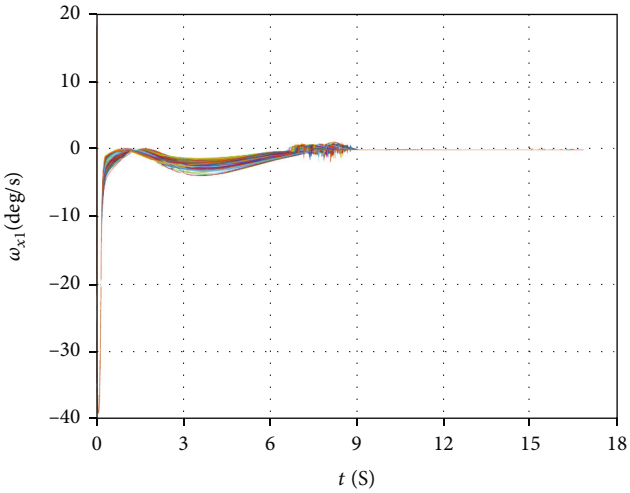

Figure 17: Roll angular rates in case 2.

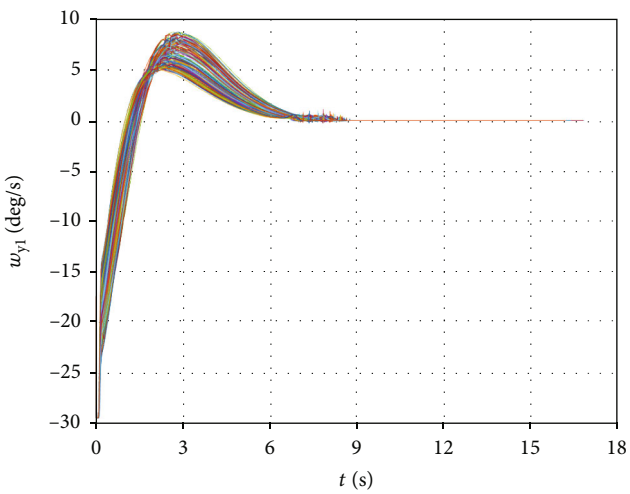

Figure 18: Yaw angular rates in case 2.

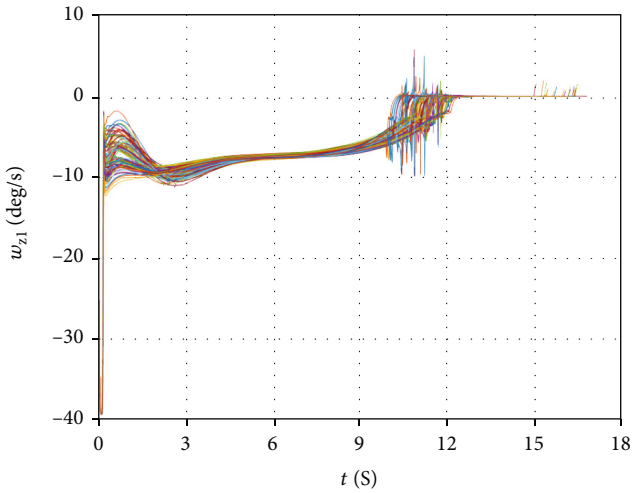

Figure 19: Pitch angular rates in case 2.

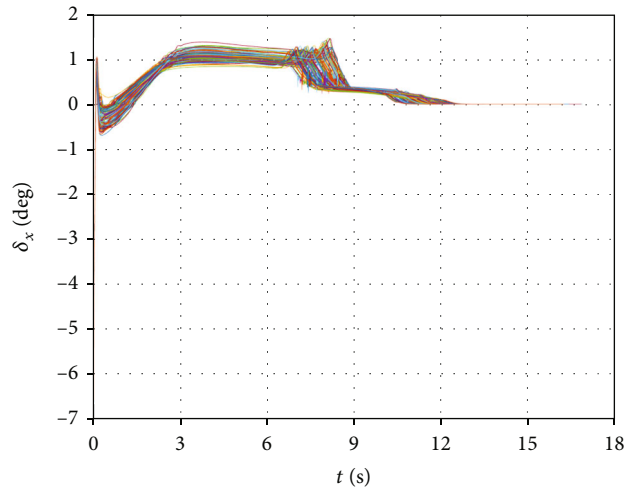

Figure 20: Roll channel rudder angles in case 2.

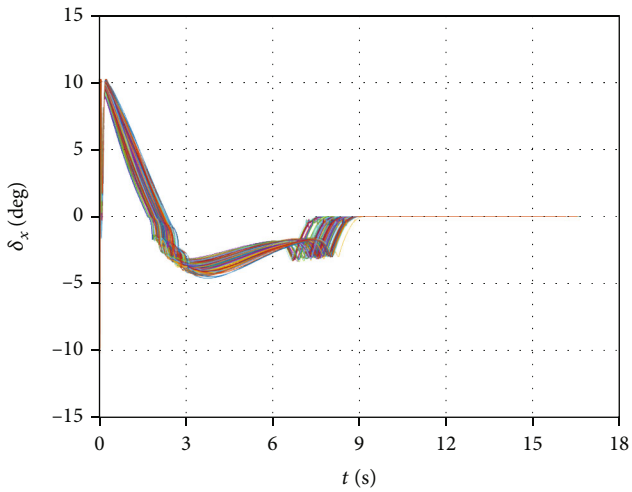

Figure 21: Yaw channel rudder angles in case 2.

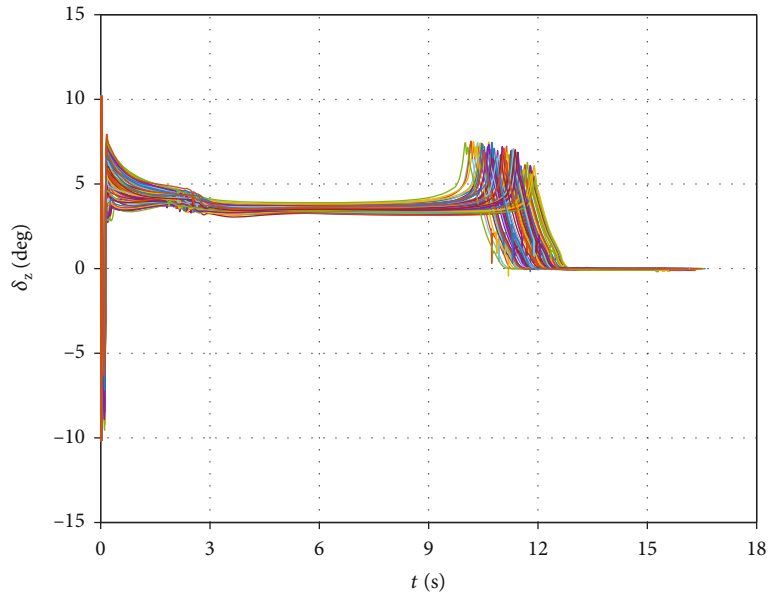

Figure 22: Pitch channel rudder angles in case 2.

The relevant aerodynamic coefficients are set as $C_{x0} = 0.32$, $C_x^{\alpha} = 0.21$, $C_x^{\beta} = 0.19$, $C_x^{\delta_x} = 0.05$, $C_x^{\delta_y} = 0.07$, and $C_x^{\delta_z} = 0.06$.

The Monte Carlo simulation results are exhibited in Figures 9–22.

As shown in Figures 9 and 10, perfect attacking target with small miss distance is achieved in each scenario. The mean and standard deviation of miss distance are found as 1.2639 m and 0.5019 m, respectively. It can be seen in Figure 11 that the missile's speed is reduced by air resistance.

In Figures 12 and 13, the LOS angles finite-time converge to the desired angles, and the convergence time is all less than t_m that embodies the fixed-time convergence characteristic of PIGC. In Figures 14–22, the system states and rudder angles are all finite-time converge to near zero and never violate the constraints. In addition, there are problems of nonsmoothness at about 10 to 11 seconds in Figures 14, 19, and 22 and at about 7 to 8 seconds in Figures 15, 16, 17, 18, 20, and 21. These were because the nonsingular terminal surface (20) proposed in this paper is a piecewise function with switching term, so when the sliding mode surface is in the switching position, the control instructions have small fluctuations; thus, the curves of the system states will appear not smooth.

It can be seen from these figures that PIGC achieves satisfactory performance under different initial fight conditions and uncertainties of the missile-related parameters. Monte Carlo simulation shows that the proposed IGC algorithm is robust.

5. Conclusion

In this paper, a novel fixed-time IGC algorithm has been proposed for terminal angle constraint, full-state constraints, and control constraint. The IGC design model considering multiple constraints is established, and the disturbance observer is used to estimate and compensate the model disturbance. The second-order instruction filter is introduced to overcome the "differential expansion," system state constraints, and control constraint. The fixed-time convergence and the stability of the IGC scheme are strictly proved. Simulation results verify the effectiveness and superiority of the proposed IGC algorithm.

The IGC algorithm proposed in this paper contains many design parameters, which can be further studied on parameter optimization.

Data Availability

All data are included within this paper.

Conflicts of Interest

The authors declare that they have no conflicts of interest.

Acknowledgments

This study was funded by the author Zhenhua Fu.

References

[1] H. Qian and T. Li, "Integrated guidance and control for missiles with three-dimensional impact angle constrained," *International Journal of Innovative Computing, Information and Control*, vol. 17, no. 2, pp. 581–593, 2021.

[2] K. Q. Zhang, L. Z. Liu, H. Ma, Z. Xu, and X. Z. Wang, "Design on integrated guidance and control considering the constraint of impact angle and input saturation," *Journal of Ballistics*, vol. 33, no. 3, pp. 9–18, 2021.

[3] H. Yan, S. P. Tan, and Y. Z. He, "A small-gain method for integrated guidance and control in terminal phase of reentry," *Acta Astronautica*, vol. 132, pp. 282–292, 2017.

[4] B. Panchal, N. Mate, and S. E. Talole, "Continuous-time predictive control-based integrated guidance and control,"

Journal of Guidance Control, and Dynamics, vol. 40, no. 7, pp. 1579–1595, 2017.

[5] L. Cui, N. Jin, and Y. T. Zong, "Guidance and control with fixed-time convergence for an interception missile," *Proceedings of the Institution of Mechanical Engineers, Part G: Journal of Aerospace Engineering*, vol. 236, no. 9, pp. 1705–1720, 2022.

[6] H. T. Song, T. Zhang, and G. L. Zhang, "L1 adaptive state feedback controller for three-dimensional integrated guidance and control of interceptor," *Proceeding of the Institution of Mechanical Engineers, Part G: Journal of Aerospace Engineering*, vol. 220, no. 10, pp. 1693–1701, 2014.

[7] S. J. Yang, J. G. Guo, and J. Zhou, "New integrated guidance and control of homing missiles with an impact angle against a ground target," *International Journal of Aerospace Engineering*, vol. 2018, Article ID 3968242, 10 pages, 2018.

[8] J. Y. Tian, N. Xiong, S. F. Zhang, H. Yang, and Z. Jiang, "Integrated guidance and control for missile with narrow field-of-view strapdown seeker," *ISA Transactions*, vol. 106, pp. 124–137, 2020.

[9] Z. H. Fu, K. Q. Zhang, Q. T. Gan, and S. Yang, "Integrated guidance and control with input saturation and impact angle constraint," *Discrete Dynamics in Nature and Society*, vol. 2020, Article ID 5917983, 19 pages, 2020.

[10] B. Zhao, S. Y. Xu, J. G. Guo, R. Jiang, and J. Zhou, "Integrated strapdown missile guidance and control based on neural network disturbance observer," *Aerospace Science and Technology*, vol. 84, pp. 170–181, 2019.

[11] L. Zhang, C. Z. Wei, R. Wu, and N. Cui, "Fixed-time extended state observer based non-singular fast terminal sliding mode control for a VTVL reusable launch vehicle," *Aerospace Science and Technology*, vol. 82, pp. 70–79, 2018.

[12] X. D. Liu, W. W. Huang, and L. F. Du, "Robust design approach of three-dimensional integrated guidance and control containing impact angle constraints," *Control Theory and Applications*, vol. 33, no. 11, pp. 1535–1542, 2016.

[13] H. Song and T. Zhang, "Fast robust integrated guidance and control design of interceptors," *IEEE Transactions on Control Systems Technology*, vol. 24, no. 1, pp. 349–356, 2016.

[14] S. Khankalantary and F. Sheikholeslam, "Robust extended state observer-based three dimensional integrated guidance and control design for interceptors with impact angle and input saturation constraints," *ISA Transactions*, vol. 104, pp. 299–309, 2020.

[15] S. Wang, W. H. Wang, and S. F. Xiong, "Impact angle constrained three-dimensional integrated guidance and control for STT missile in the presence of input saturation," *ISA Transactions*, vol. 64, pp. 151–160, 2016.

[16] W. K. Liu, Y. Y. Wei, M. Z. Hou, and G. Duan, "Integrated guidance and control with partial state constraints and actuator faults," *Journal of the Franklin Institute*, vol. 356, no. 9, pp. 4785–4810, 2019.

[17] C. Zhenyu, G. Jianguo, Z. Bin, G. Zongyi, and L. Xiaodong, "Finite-time integrated guidance and control system for hypersonic vehicles," *Transactions of the Institute of Measurement and Control*, vol. 43, no. 4, pp. 842–853, 2021.

[18] S. M. He, W. Wang, and J. Wang, "Three-dimensional multivariable integrated guidance and control design for maneuvering targets interception," *Journal of the Franklin Institute-Engineering and Applied Mathematics*, vol. 353, no. 16, pp. 4330–4350, 2016.

[19] Y. J. Shu and S. Tang, "Integrated guidance and control backstepping design for blended control missile based on NDO," *Journal of Astronautics*, vol. 34, no. 1, pp. 79–85, 2013.

[20] X. D. Liu, W. W. Huang, and L. F. Du, "An integrated guidance and control approach in three-dimensional space for hypersonic missile constrained by impact angles," *ISA Transactions*, vol. 66, pp. 164–175, 2017.

[21] S. M. He, D. F. Lin, and J. Wang, "Continuous second-order sliding mode based impact angle guidance law," *Aerospace Science and Technology*, vol. 41, pp. 199–208, 2015.

[22] J. K. Ni, L. Liu, C. X. Liu, X. Hu, and T. Shen, "Fixed-time dynamic surface high-order sliding mode control for chaotic oscillation in power system," *Nonlinear Dynamics*, vol. 86, no. 1, pp. 401–420, 2016.

[23] X. Wang, J. Guo, S. J. Tang, and S. Qi, "Fixed-time disturbance observer based fixed-time back-stepping control for an air-breathing hypersonic vehicle," *ISA Transactions*, vol. 88, pp. 233–245, 2019.

[24] B. Y. Jiang, Q. L. Hu, and M. I. Friswell, "Fixed-time attitude control for rigid spacecraft with actuator saturation and faults," *IEEE Transactions on Control Systems Technology*, vol. 24, no. 5, pp. 1892–1898, 2016.

[25] M. Basin, C. B. Panathula, and Y. Shtessel, "Multivariable continuous fixed-time second-order sliding mode control: design and convergence time estimation," *IET Control Theory & Applications*, vol. 11, no. 8, pp. 1104–1111, 2017.

[26] K. Q. Zhang, S. C. Yang, B. C. Li, and C. Liu, "Fixed-time convergent guidance law considering autopilot dynamics," *Acta Aeronautica et Astronautica Sinica*, vol. 40, no. 11, article 323227, 2019.